Available online at www.sciencedirect.com
SCIENCE DIRECT
Journal of Catalysis 238 (2006) 177–185
JOURNAL OF CATALYSIS
www.elsevier.com/locate/jcat

# Gold nanoparticles dispersed polyaniline grafted multiwall carbon nanotubes as newer electrocatalysts: Preparation and performances for methanol oxidation

P. Santhosh [a], A. Gopalan [a,b,c], Kwang-Pill Lee [a,b,*]

[a] *Advanced Analytical Science and Nanomaterials Laboratory, Department of Chemistry Education, Kyungpook National University, Daegu 702-701, South Korea*
[b] *Nano Practical Application Center, Daegu 702-230, South Korea*
[c] *Department of Industrial Chemistry, Alagappa University, Karaikudi-630003, India*

Received 8 October 2005; revised 27 November 2005; accepted 6 December 2005

Available online 9 January 2006

**Abstract**

Newer electrocatalysts were prepared by dispersing gold nanoparticles onto a polyaniline (PANI) grafted multiwall carbon nanotube (MWNT-g-PANI) matrix through a two-step electrochemical process. In the first step, PANI chains were grafted onto amine-functionalized MWNT (MWNT-$NH_2$) by electropolymerizing a mixture of aniline and MWNT-$NH_2$ (dispersed in cetyltrimethyl ammonium bromide) using cyclic voltammetry. In the second step, Au nanoparticles were dispersed into the film of MWNT-g-PANI by electrochemical reduction of $HAuCl_4$. MWNT-g-PANI-modified electrodes with varying amounts of Au nanoparticles were prepared. Films of MWNT-g-PANI-Au were analyzed by field emission transmission electron microscopy (FETEM). The FETEM images indicate that Au particles of 8–10 nm in size are uniformly distributed into MWNT-g-PANI. X-Ray diffraction patterns provide support for the existence of Au nanoparticles. The electrocatalytic properties of the MWNT-g-PANI-Au electrode toward oxidation of methanol and adsorbed carbon monoxide ($CO_{ads}$) were investigated by chronoamperometry and $CO_{ads}$ stripping voltammetry and compared with the properties of MWNT-Au and pristine Au electrodes. MWNT-g-PANI-Au catalysts exhibit excellent electrocatalytic activity toward the oxidation of methanol and $CO_{ads}$. Oxidation of methanol occurs at a much lower oxidation potential (780 mV) at the MWNT-g-PANI-Au electrode with high current densities compared with the MWNT-Au electrode (890 mV) and pristine Au electrode (930 mV), due to the dispersion of Au nanoparticles into the three-dimensional network of MWNT-g-PANI. Further, our results suggest that the MWNT-g-PANI-Au electrode has better oxidation kinetics for the oxidation of $CO_{ads}$ to $CO_2$ than the MWNT-Au and pristine Au electrodes. Our results indicate that the MWNT-g-PANI-Au catalyst can have potential applications in direct methanol fuel cells.


*Keywords:* Electrocatalyst; Gold nanoparticles; Carbon nanotubes; Chronoamperometry; Stripping voltammetry

## 1. Introduction

Investigations aiming at developing efficient fuel cells have contributed greatly to the development of catalysts for the electrooxidation of small organic molecules. Among these molecules, methanol has been the most widely investigated, due to its possible use as a fuel in direct methanol fuel cells (DMFCs). Platinum and platinum-based catalysts are known to activate the dissociative adsorption of methanol at an appreciable rate in acid medium. The main concern in the catalysis process is the possible formation of self-poisoning species, strongly adsorbed carbon monoxide ($CO_{ads}$), at the platinum surface [1–4]. Adsorption of CO on the electrode surface blocks the active sites in the electrocatalyst and results in an overpotential for methanol oxidation, ultimately resulting in decreased cell voltage and low power densities for DMFCs.

Recently, gold catalysts have been reported to have promising applications in the oxidation of methanol. Au nanoparticle (<10 nm)-loaded electrodes have demonstrated high catalytic activity for both oxidation and reduction reactions [5–8]. The

* Corresponding author. Fax: +82 539528104.
*E-mail addresses:* algopal_99@yahoo.com (A. Gopalan), kplee@knu.ac.kr (K.-P. Lee).

0021-9517/$ – see front matter 
doi:10.1016/j.jcat.2005.12.014

advantage of Au over Pt and Pt-based alloys is that during methanol electrooxidation, intermediates that can cause poisoning of catalyst are not formed [9]. Also, Au-based catalysts offer an economic advantage over Pt-based catalysts [10]. Haruta et al. [10] demonstrated that well-dispersed nanosized Au catalysts are extremely active for CO oxidation and thus can be suitable for minimizing the poisoning effect of $CO_{ads}$ at the catalyst surface. The optimum Au particle size in the catalyst system seems to be around 3 nm [11,12]. The catalytic behaviour is rather complex and depends on the size of the Au particles [11,12], the type of support [13,14], and the methods of catalyst preparation [15]. Consequently, it is highly desirable to fabricate catalysts with a higher loading of uniform-sized Au nanoparticles [16].

The dispersion of catalyst particles on the substrate determines the catalyst's performance as an electrode material [17]. It has been reported that an effective dispersion of catalyst particles causes a decrease in surface poisoning [18,19]. Different substrates have been tried for the dispersion of catalyst particles with the aim of improving the efficiency of methanol electrooxidation [20–23].

Carbon nanotubes (CNTs) have attracted much interest from fundamental and applied perspectives, owing to their good mechanical and unique electrical properties [24]. CNTs are considered the potential supports for making heterogeneous catalysts [25–27]. Electrocatalysts with Pt nanoparticles loaded onto carbon tubule membranes [28] and highly ordered nanoporous arrays of carbon [29] have been proven effective for oxidation-reduction reactions. However, there are difficulties in dispersing metal nanoparticles with uniform dispersion and regular sizes at the CNT surfaces. To obtain a good particle size monodispersity for nanoparticle dispersion, the surface of CNT must be modified via proper functionalization.

Conducting polymers have proven the suitable host matrices for dispersing metallic particles. The composites of conducting polymer with metal nanoparticles permit a facile flow of electronic charges through the polymer matrix during electrochemical processes. Conducting polymer plays additional roles in electrochemical processes. The conducting polymer provides a low ohmic drop to the bulk and limits mass transfer for the electroactive species to reach the catalytic sites. Also, metallic particles could be dispersed into the matrix of these polymers. Through a suitable combination of conducting polymer and metal nanoparticles, newer electrodes could be generated with higher surface areas and enhanced electrocatalytic activities toward the oxidation of methanol [23,30].

In the present study, we developed a novel catalyst comprising multiwall carbon nanotube (MWNT), conducting polymer, and gold nanoparticles. MWNT was suitably functionalized and further used to form grafted chains of polyaniline (PANI) through electrochemical polymerization. Au nanoparticles were electrochemically dispersed into the matrix of PANI-grafted MWNT. For the purposes of comparison, catalysts were also prepared by loading Au particles into functionalized MWNT. The newer catalysts thus formed were characterized by X-ray diffraction (XRD) and field emission transmission microscopy (FETEM). The electroactivity of the catalysts toward oxidation of methanol and CO were evaluated to ascertain the utility of these catalysts for applications in DMFCs.

## 2. Experimental

### 2.1. Reagents

Aniline (Aldrich) was distilled and used. Multiwall carbon nanotubes, MWNT (10–50 nm diameter) obtained from CNT (Incheon, Korea) were rinsed with double-distilled water and dried. Poly(ethylene glycol) bis(3-aminopropyl) terminated, nitric acid, thionly chloride, THF, cetyltrimethyl ammonium bromide, auric acid, methanol, and perchloric acid (analytical grade; Aldrich) were used as received.

### 2.2. Functionalization of MWNT

The following procedure was adopted for the preparation of amine-functionalized MWNTs (Scheme 1A). First, 50 mg of MWNT was refluxed in 4 M $HNO_3$ for 24 h and filtered through a polycarbonate membrane (0.2 μm pore size). The residue, MWNT-COOH (carboxylated MWNT), was washed with deionized water and dried under vacuum at 60 °C for 12 h. Then 50 mg of MWNT-COOH was refluxed in 100 mL of thionyl chloride at 65 °C for 24 h to obtain MWNT-COCl. The MWNT-COCl was filtered, washed with THF, and dried under vacuum at room temperature. Amine-functionalized MWNT was prepared by refluxing MWNT-COCl with poly(ethylene glycol) bis(3-aminopropyl) terminated in THF at 60 °C for 24 h. The amine-functionalized MWNT (MWNT-$NH_2$) was separated by filtration and dried under vacuum.

### 2.3. Fabrication of MWNT-g-PANI-Au electrode

Cyclic voltammetry was used to deposit MWNT-g-PANI as a film on the surface of the Au electrode to obtain a MWNT-g-PANI–modified electrode (Scheme 1B). The preparation of this MWNT-g-PANI–modified electrode was fabricated as follows. First, 50 mg of MWNT-$NH_2$ was dispersed in 0.5 M cetyltrimethyl ammonium bromide (CTAB) by applying ultrasonication (BRANSON Digital Sonifier) for 3 h; then 10 mM aniline was dissolved in this solution. The solution containing MWNT-$NH_2$ and aniline was subjected to electrochemical polymerization by continuous potential cycling in the potential range of 0–900 mV. A green-colored deposit (MWNT-g-PANI) was seen on the surface of the electrode. After deposition, the Au electrode coated with MWNT-g-PANI was washed with water and stored under nitrogen atmosphere. Au particles were electrochemically deposited onto the MWNT-g-PANI film from a 0.5 M $H_2SO_4$ solution of $HAuCl_4$ using a repetitive potential scan from 1.1 to 0.0 V (vs. saturated calomel electrode [SCE]), and MWNT-g-PANI-Au electrode was fabricated.

### 2.4. Fabrication of MWNT-$NH_2$-Au electrode

A black suspension (MWNT-$NH_2$) was prepared by dispersing 50 mg of MWNT-$NH_2$ in 0.5 M CTAB with the aid

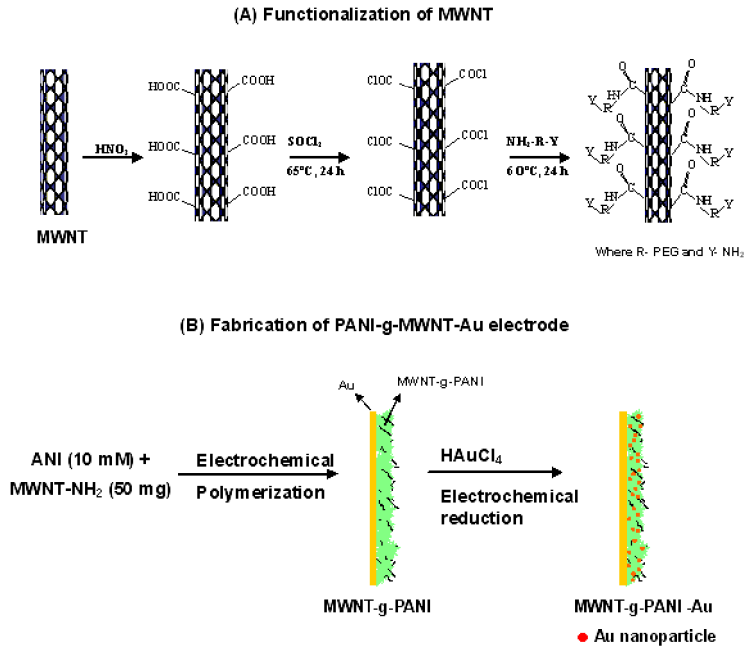


Scheme 1.

of ultrasonication. About 1.0 μL of the black suspension was dropped on the surface of the Au electrode and kept at 60 °C for 12 h to evaporate the solvent. The Au electrode coated with MWNT-$NH_2$ was washed with water and stored under nitrogen atmosphere. Au particles were electrochemically deposited onto the MWNT-$NH_2$ surface by adopting the procedure detailed earlier to fabricate an Au nanoparticle-dispersed MWNT-$NH_2$ electrode.

### 2.5. Instrumentation

Electrochemical measurements were performed using an EG & G PAR 283 electrochemical analyzer. A three-compartment cell, in which the reference electrode was separated from the working and counter electrode compartments by a Luggin capillary, was used for the electrochemical studies. Potentials are reported versus the SCE. A Ds-Advanced Burker AXS diffractometer with a Cu-$K_\alpha$ source was used to obtain XRD spectra of the catalysts. The spectra were scanned in the range $2\theta = 0°$–$80°$. The morphology of the catalyst was examined by FETEM using a JOEL JEM-2000EX with a field emission gun operated at 200 kV.

### 2.6. Electrochemical studies

Methanol oxidation studies were carried out using 1 M $CH_3OH$ + 0.1 M $HClO_4$. Before the electrochemical studies, the solutions were deoxygenated using high-purity argon gas. Electrocatalytic activity of the electrodes toward methanol oxidation was evaluated by using cyclic voltammetry and chronoamperometry measurements. For cyclic voltammetric measurements, potentials were scanned between −0.15 and 1.1 V versus SCE, at a scan rate of 100 mV $s^{-1}$. Chronoamperometric measurements were carried out to obtain current-time curves at different potentiostatic conditions (0.8 and 1.2 V). Voltammetric measurements were performed under continuous bubbling of CO, to monitor the poisoning effect of CO. First, CO was adsorbed onto the catalyst electrode that was kept at 0.10 V by bubbling CO gas through the 0.1 M $HClO_4$ solution for 20 min. Residual CO in the solution was subsequently removed by bubbling high-purity Ar gas while holding the potential at 0.10 V. The potential was then cycled at a scan rate of 5 mV $s^{-1}$. Double-distilled water was used throughout the experiments. All experiments were carried out at room temperature unless stated otherwise.

## 3. Results and discussion

### 3.1. Fabrication of electrodes

#### 3.1.1. Gold nanoparticle-dispersed MWNT-g-PANI electrode

Modification of the surface of working electrode (Au) was performed in two steps. In the first step, MWNT-g-PANI film was deposited onto the working electrode (Au) using cyclic voltammetry. In the second step, Au nanoparticles were incorporated into MWNT-g-PANI film by electrochemical reduction of $HAuCl_4$.

Fig. 1 displays the cyclic voltammograms (CVs) recorded during electropolymerization. The formation of MWNT-g-PANI film was evident from the cyclic voltammetric findings. In the first potential cycle, a significantly higher peak current at the potential of aniline oxidation was noted for the solution containing MWNT-$NH_2$ and aniline than for the solution containing aniline alone. This gives a clue that the amine groups in MWNT-$NH_2$ and aniline were simultaneously oxidized at the potential of aniline oxidation. Consequently, a cross-reaction could occur between the amine cation radicals formed from MWNT-$NH_2$ and aniline. This was considered the nucleation

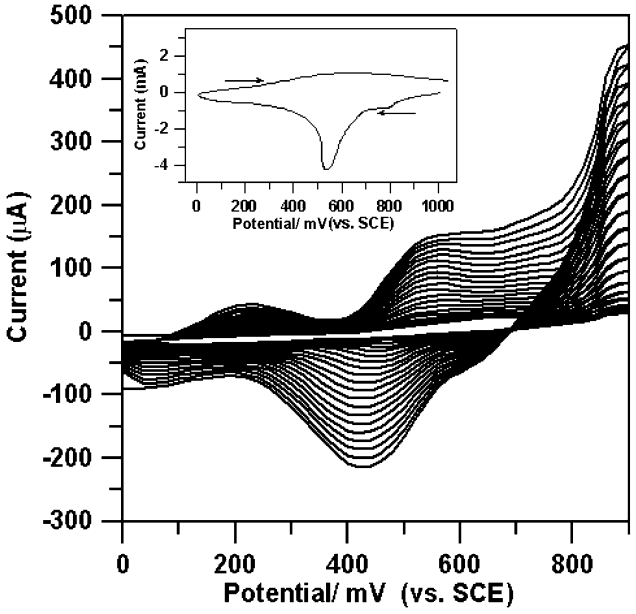


Fig. 1. Cyclic voltammograms recorded during the electrochemical polymerization of the solution containing 10 mM aniline and 50 mg poly(ethyleneglycol) bis(3-ammopropyl) functionalized MWNT. (Inset: cyclic voltammetry of $2.0 \times 10^{-4}$ M $AuCl_4^-$ in 0.5 M $H_2SO_4$ at MWNT-g-PANI electrode, scan rate: 100 mV $s^{-1}$.)

step for grafting of PANI onto MWNT. Moreover, current values at the redox peaks corresponding to PANI (Fig. 1) showed a continuous increase with the number of potential cycles. Further, position of redox peaks of MWNT-g-PANI was found to be different compared with simple PANI. For example, the transformation of leucoemeraldin state to emeraldin state occurs at a lower potential (200 mV) for the MWNT-g-PANI compared with simple PANI (220 mV) [31,32]. Transformation of emeraldin state to a further oxidized form also occurred at a different potential for MWNT-g-PANI than for simple PANI [31]. These observations indicate the buildup of MWNT-g-PANI film on the Au electrode surface. The forgoing cyclic voltammetric results on the electropolymerization of a mixture of MWNT-$NH_2$ and aniline clearly demonstrate that a MWNT-g-PANI film was formed on the surface of working electrode (Au). Fig. 1 (inset) shows the current potential curve for the reduction of $HAuCl_4$ at the MWNT-g-PANI electrode. Two cathodic peaks can be seen at ∼0.80 and ∼0.53 V. The sharp peak at 0.53 V represents the reduction of solution-bound $Au^{III}$ to $Au^0$ [33], and the initial wave at 0.80 V is attributed to the reduction of adsorbed $AuCl_4^-$ ions to $Au^0$ [33]. A similar voltammetric response has been reported for the adsorption of Au complexes to carbon electrodes and consequent formation of $Au^0$ [34,35]. Furthermore, no anodic current was observed on the reverse sweep, indicating that $Au^0$ nanoparticles were irreversibly present in the MWNT-g-PANI matrix. It is important to note that the reduction of $HAuCl_4$ at the MWNT-g-PANI electrode occurs with an overpotential of ∼300 mV compared with that observed at the bare Au electrode. Incorporation of $Au^0$ nanoparticles into MWNT-g-PANI film resulted in the new modified MWNT-g-PANI-Au electrode.

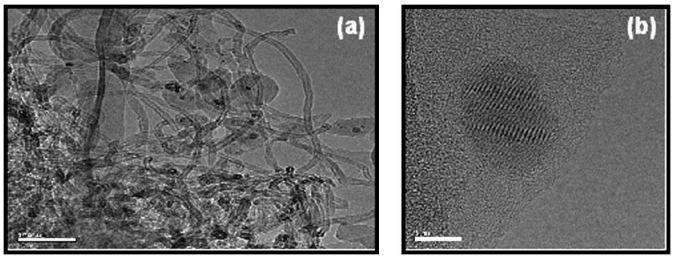


Fig. 2. FETEM images MWNT-g-PANI-Au electrode (20 μg Au $cm^{-2}$) and (b) magnified part of one gold nanoparticle.

### 3.1.2. Gold nanoparticle-dispersed MWNT-$NH_2$ catalyst

Au nanoparticles were deposited onto simple MWNT-$NH_2$ electrode (described in the Experimental section) under the identical conditions as used for the incorporation of Au nanoparticles into MWNT-g-PANI matrix. Two cathodic peaks were observed at 0.82 and 0.50 V, corresponding to the reduction of adsorbed $AuCl_4^-$ ions to $Au^0$ and reduction of solution-bound $Au^{III}$ to $Au^0$, respectively.

## 3.2. Characterization of MWNT-g-PANI-Au and MWNT-$NH_2$-Au catalyst

FETEM images of MWNT-g-PANI-Au (Fig. 2) clearly show that $Au^0$ nanoparticles with an average size of ∼8–10 nm are distributed into MWNT-g-PANI surface. These FETEM images also reveal the presence of PANI over the entire surface of MWNT at a thickness of about 10–15 nm. Keep in mind that previous reports on dispersion of metal particles (Pt) onto carbon nanotubes did not describe such a uniform dispersion of smaller-sized metal nanoparticles [36,37], possibly due to the formation of Pt particles at the defect sites. In the present study, we functionalized MWNT with the poly(ethylene glycol) bis(3-aminopropyl) terminated group (MWNT-$NH_2$) for two reasons: (1) the amine group in MWNT-$NH_2$ augments the grafting of PANI chains through covalent linkages, and the long poly(ethylene glycol) chain may cover the defect sites in MWNT; and (2) grafting of PANI on MWNT surfaces also masks the defect sites in MWNT and provides a uniform surface with positively charged (protonated amine/imine) sites. The positive charges from the aniline (amine/imine) units in PANI electrostatically absorb gold ions, creating a sink of gold ions in the matrix. Au nanoparticle formation is expected to occur at the adsorbed sites, hence avoiding aggregation. The specific electrostatic interaction between the sites in PANI and adsorbed $Au^0$ produces a narrow particle size distribution without causing random nucleation [38].

Different amounts of $Au^0$ nanoparticles were dispersed onto MWNT-g-PANI and simple MWNT-$NH_2$ matrices. The amount of $Au^0$ nanoparticles deposited in MWNT-g-PANI or MWNT-$NH_2$ electrodes was calculated from the following equation:

$$m = \frac{Q_{\text{dep}} M}{F Z},$$

where $Q_{\text{dep}}$ (obtained through graphical integration of cyclic voltammetric curves) is the charge used for the deposition

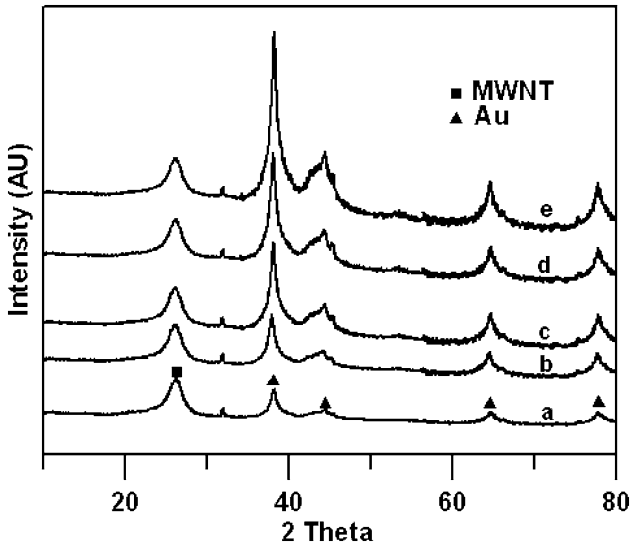


Fig. 3. XRD patterns of MWNT-g-PANI with different amount of electrodeposited Au nanoparticles: (a) 5, (b) 10, (c) 20, (d) 30, and (e) 40 μg cm$^{-2}$.

of Au, $M$ is the molecular weight of Au, $F$ is the Faradic constant, and $Z$ is the number of electrons transferred (here taken as 3) for the formation of $Au^0$. Electrodes with similar amounts of $Au^0$ in MWNT-g-PANI and MWNT-$NH_2$ electrodes were fabricated.

The crystalline structure and size of the Au particles deposited on the MWNT-g-PANI electrode were examined by XRD analysis. XRD patterns of MWNT-g-PANI containing different amounts of $Au^0$ nanoparticles are presented in Fig. 3. XRD patterns of MWNT-g-PANI-Au with $Au^0$ nanoparticles loaded in the range of 5–40 μg cm$^{-2}$ (Fig. 3a–e) show Bragg reflection patterns at $2\theta \approx 38°$ (111), 44° (200), 65° (220), and 78° (311), indexed for the face-centered cubic (fcc) structure of gold particles [39]. Further, a diffraction peak at $2\theta \approx 27°$ corresponding to the (002) G phase of MWNT or graphite [40] also coexists. It is important to note that the intensities of the $2\theta$ values related to $Au^0$ particles increase with increasing $Au^0$ amount. From the full width measured at the half-maximum of the peak at $2\theta = 38°$, the crystallite size of the Au particles was evaluated using Scherer's equation [41]. The average crystallite size as determined through Scherer's equation (5–8 nm) is close to that observed by FETEM.

### 3.3. Electrooxidation of methanol using the catalyst electrodes

#### 3.3.1. Cyclic voltammetry studies

The electrocatalytic activity of $Au^0$ nanoparticle-loaded MWNT-g-PANI (MWNT-g-PANI-Au) electrodes was evaluated for methanol oxidation by cyclic voltammetry and compared with Au nanoparticle-loaded MWNT-$NH_2$ (MWNT-Au) and pristine Au electrodes. The dotted and solid curves in Fig. 4 show the CVs of electrooxidation of methanol at (a) MWNT-g-PANI-Au (Au loading, 30 μg cm$^{-2}$), (b) MWNT-Au (Au loading, 30 μg cm$^{-2}$), and (c) pristine Au electrodes in 0.1 M $HClO_4$ and 0.1 $HClO_4$ + 1 M $CH_3OH$ solutions, respectively. Comparing the curves in Fig. 3a–c demonstrates that the MWNT-g-PANI-Au and MWNT-Au electrodes are catalytically more

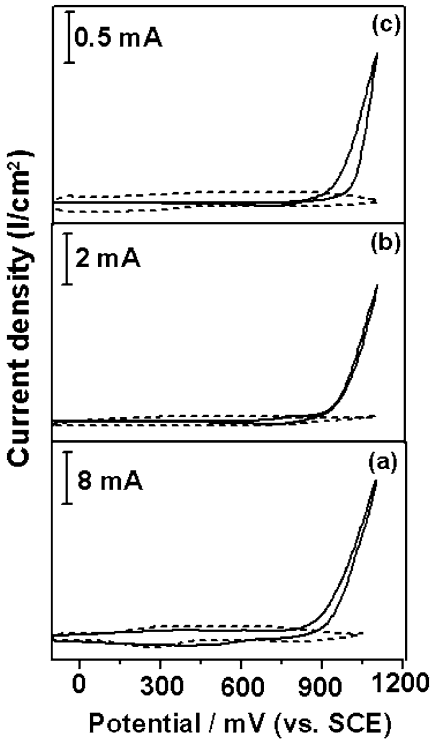


Fig. 4. Cyclic voltammograms of (a) MWNT-g-PANI-Au, (b) MWNT-Au (Au loading 30 μg cm$^{-2}$), and (c) pristine Au electrode in 0.1 M $HClO_4$ (- - -, absence of methanol; —, presence of 1 M $CH_3OH$).

active than the pristine Au electrode. The results also clearly reveal that the MWNT-g-PANI-Au electrode has significantly greater electrocatalytic activity than the other electrodes. For example, at the anodic potential of 1.1 V, the MWNT-g-PANI-Au electrode has a current density of about 28.3 mA cm$^{-2}$, nearly four times higher than that of the MWNT-Au electrode (6.8 mA cm$^{-2}$). Further, methanol oxidation occurs at a much lower oxidation potential (780 mV) at the MWNT-g-PANI-Au electrode than at the MWNT-Au electrode (890 mV) and pristine Au electrode (930 mV). Obviously, the enhanced catalytic activity for methanol oxidation for MWNT-g-PANI-Au and MWNT-Au electrodes arises from the existence of Au nanoparticles distributed in MWNT-g-PANI and MWNT matrices, respectively. Nonetheless, the enhanced catalytic activity for methanol oxidation cannot be correlated to the actual surface area of Au nanoparticles, due to the absence or negligible presence of hydrogen adsorption/desorption peaks at MWNT-g-PANI-Au and MWNT-Au electrodes.

We hypothecate two main reasons for the enhanced electrocatalytic activity toward methanol oxidation of the MWNT-g-PANI-Au electrode compared with other electrodes: the crystallite size of Au nanoparticles and the distribution of Au nanoparticles in the matrix. A high surface area of Au particles is anticipated due to the uniform distribution of Au nanoparticles in the three-dimensional MWNT-g-PANI network. Moreover, the presence of PANI as a grafted chain onto MWNT electrostatically stabilizes the Au nanoparticles and prevents aggregation of particles. As a result, smaller particles of Au can be distributed in the MWNT-g-PANI matrix. The presence of

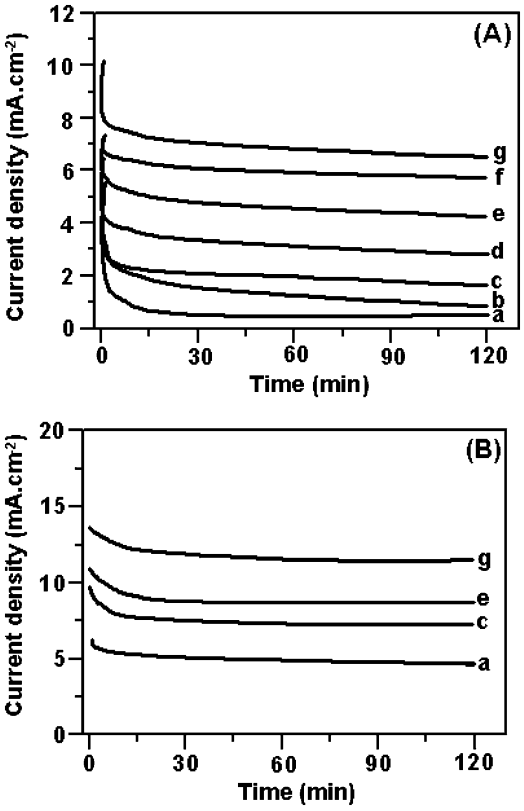


Fig. 5. Chronoamperometric response of MWNT-g-PANI-Au electrode polarized at 1.2 V (A) and 0.8 V (B) in 0.1 M $HClO_4$ and 1 M $CH_3OH$. Amount of gold nanoparticles loaded: (a) 5, (b) 10, (c) 20, (d) 30, (e) 40, (f) 50, and (g) 60 μg $cm^{-2}$.

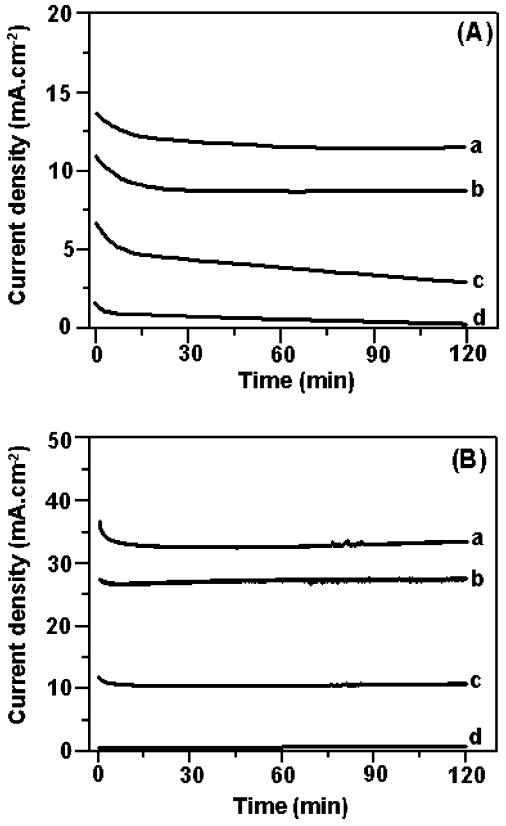


Fig. 6. Chronoamperometric response of (a) and (b) MWNT-g-PANI-Au electrodes (Au loading 40 and 60 μg $cm^{-2}$, respectively), (c) MWNT-Au (Au loading 60 μg $cm^{-2}$) and (d) pristine Au electrode polarized at 0.8 V in 0.1 M $HClO_4$ and 1 M $CH_3OH$; at 25 °C (A) and 60 °C (B).

larger (>15 nm) Au nanoparticles in the MWNT-$NH_2$ matrix may be due to the absence of the stabilization influence and three-dimensional network structure present in the MWNT-g-PANI electrode. The presence of PANI on the MWNT surface provides positively charged sites to $AuCl_4^-$ anions [42]. The $Au^0$ nanoparticles formed at these sites show a lower tendency to aggregate on the MWNT-g-PANI surface. Dalmia et al. [43] demonstrated the feasibility of synthesizing nanometer-sized Pt particles using a negatively charged polymer, poly(N-sulfonatopropyl *p*-benzamide). The synthesis of nanometer-sized Pt colloids using polyacrylic acid also has been reported [44,45].

### 3.3.2. *Chronoamperometric analysis*

The electrocatalytic activity of the MWNT-g-PANI-Au electrodes toward electrooxidation of methanol was systematically evaluated through chronoamperometry in a 1 M methanol/0.1 M $HClO_4$ solution by polarizing at 1.2 and 0.8 V. Figs. 5A and B show chronoamperometric responses for MWNT-g-PANI electrode loaded with different amounts (5–60 μg $cm^{-2}$) of $Au^0$ nanoparticles, polarized at 1.2 and 0.8 V, respectively. The PANI-g-MWNT-Au electrode with a greater amount of Au nanoparticles exhibits a higher current value. Obviously, an increase in the surface area of $Au^0$ nanoparticles enhances electroactivity. A similar result has been reported for Pt nanoparticles deposited on tin oxide/tin electrodes [46]. The current densities are also dependent on the use of polarization voltage. Whereas the chronoamperometric response for the electrode polarized at 0.8 V was stable over the period of polarization (Fig. 5B), a decay in the current over time was noted for the MWNT-g-PANI-Au electrode polarized at 1.2 V. These results indicate that the MWNT-g-PANI-Au electrode polarized with 1.2 V deactivates at a faster rate. We therefore conclude that the MWNT-g-PANI-Au electrode polarized at 0.8 V has better electrocatalytic activity for methanol oxidation.

The electrocatalytic activity of MWNT-g-PANI-Au electrode containing 60 μg $cm^{-2}$ of electrodeposited $Au^0$ nanoparticles for the electrooxidation of methanol was compared to the activity of MWNT-Au electrode containing the same amount of electrodeposited $Au^0$ nanoparticles and also with pristine Au electrode. The chronoamperometric curves (Fig. 6A) obtained for these electrodes, polarized at 0.8 V, clearly indicate that the MWNT-g-PANI-Au electrode has greater electroactivity than the MWNT-Au and pristine Au electrodes. After 60 min of polarization at 0.8 V (at 25 °C), the MWNT-g-PANI-Au electrode had a current density of approximately 12 mA $cm^{-2}$, compared with current densities of approximately 4.8 mA $cm^{-2}$ for the MWNT-Au electrode and 3 mA $cm^{-2}$ for the pristine Au electrode. Moreover, the current value of electrooxidation decayed faster for the MWNT-Au electrode (Fig. 6A-c) than for the MWNT-g-PANI-Au electrode (Fig. 6A-a and b).

We also tested the performance of the electrodes at a temperature of 60 °C. Fig. 6B presents the chronoamperometric

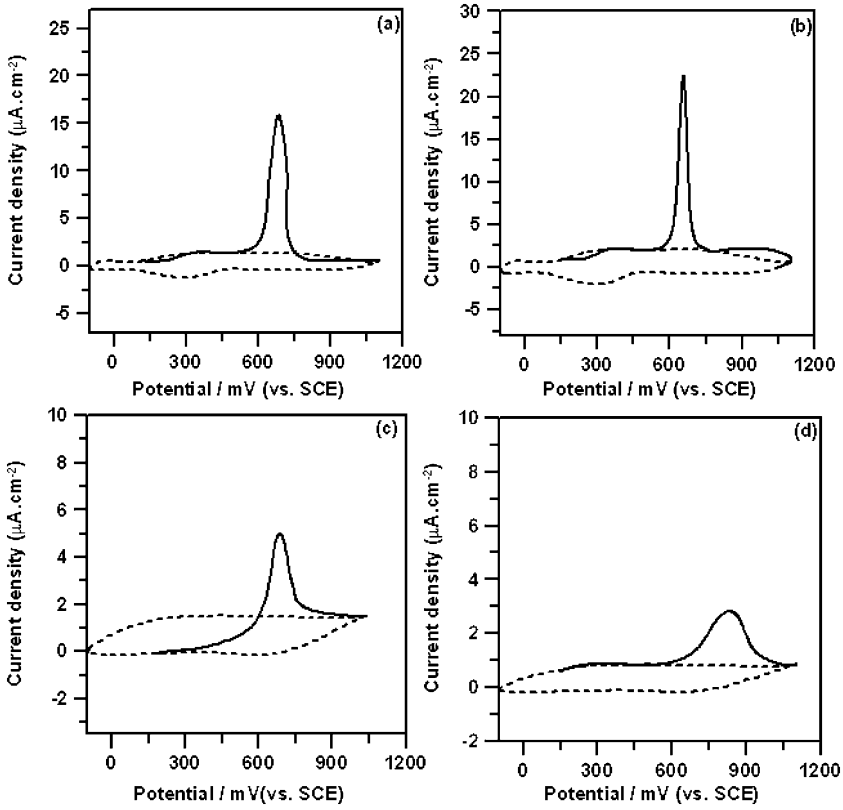


Fig. 7. $CO_{ads}$ stripping voltamograms recorded at 5 mV $s^{-1}$ in 0.1 M $HClO_4$. The CO was adsorbed at 0.1 V for 20 min, subsequently, the solution CO was removed. —, $CO_{ads}$ stripping voltammogram; - - -, second cycle (background CV) in 0.1 M $HClO_4$. (a) and (b) MWNT-g-PANI-Au electrode (Au loading 40 and 60 μg $cm^{-2}$, respectively), (c) MWNT-Au (Au loading 60 μg $cm^{-2}$), and (d) pristine Au electrode.

curves obtained for these electrodes polarized at 0.8 V at 60 °C. A rise in current densities occurred with an increase in temperature from 25 to 60 °C. The current density is higher at 60 °C for MWNT-g-PANI-Au (32 mA $cm^{-2}$) and MWNT-Au (11 mA $cm^{-2}$) electrodes (with equal amounts of Au nanoparticles) compared with pristine Au electrode (1.2 mA $cm^{-2}$). The oscillations observed in the chronoamperometric curves registered at 60 °C are due to the release of $CO_2$ bubbles [47]. The $OH_{ads}$ formed by dehydrogenation of water reacts with the adsorbed CO to produce $CO_2$ gas, which can cause release of blocked sites (by $CO_{ads}$) of catalyst and subsequently an increased free surface area.

### 3.4. $CO_{ads}$-Stripping voltammetry

Generally, CO formed as a byproduct during the electrooxidation of methanol strongly adsorbs on the noble metal catalyst (anode) and subsequently suppresses the methanol oxidation reaction. This poisoning effect of CO leads to decreased anode performance. Consequently, generation of a CO-tolerant catalyst has been a priority for the successful development of more efficient fuel cell systems. $CO_{ads}$-stripping voltammetry can yield useful in situ electrochemical information about the electroactivity of the Au catalyst surfaces in the electrochemical environment and has been used as a probe for monitoring the surface composition of many alloys [48]. Figs. 7a-d shows typical $CO_{ads}$-stripping voltammograms recorded at 5 mV $s^{-1}$ in 0.1 M $HClO_4$. Table 1 summarizes various electrochemical parameters, the onset potential ($E_{on}$) for the $CO_{ads}$ to $CO_2$ oxidation reaction, and the peak width of the $CO_{ads}$ stripping peaks measured as full width at half height of the peak ($E_{FWHM}$), extracted from voltammograms. As can be seen from Fig. 7 and Table 1, lower onset potential for the oxidation of $CO_{ads}$ is observed at the MWNT-g-PANI-Au electrode compared with the pristine Au electrode (Table 1). This may be due to the bifunctional mechanism that may be operating at MWNT-g-PANI-Au electrodes. In this mechanism, the dehydrogenation of water forms Au–$OH_{ads}$, which can combine with adsorbed CO and remove CO from the surface. These reactions are supposed to be catalyzed by the $Au^0$ nanoparticles present in three-dimensional matrix of PANI.

Table 1
Comparative performance of electrodes from $CO_{ads}$ stripping voltammetry

| Catalyst | $E_{on}$ (V) | $E_{pa}$ (V) | $E_{FWHM}$ (mV) |
|---|---|---|---|
| MWNT-g-PANI-Au (Au-40 μg $cm^{-2}$) | 0.52 | 0.69 | 125 |
| MWNT-g-PANI-Au (Au-60 μg $cm^{-2}$) | 0.50 | 0.65 | 75 |
| MWNT-Au (Au-60 μg $cm^{-2}$) | 0.58 | 0.70 | 175 |
| Au | 0.60 | 0.85 | 208 |

$E_{on}$, onset potential for the $CO_{ads}$ to $CO_2$ oxidation; $E_{pa}$, anodic peak for the $CO_{ads}$ to $CO_2$ oxidation; $E_{FWHM}$, full width at half height of $CO_{ads}$ stripping peak.

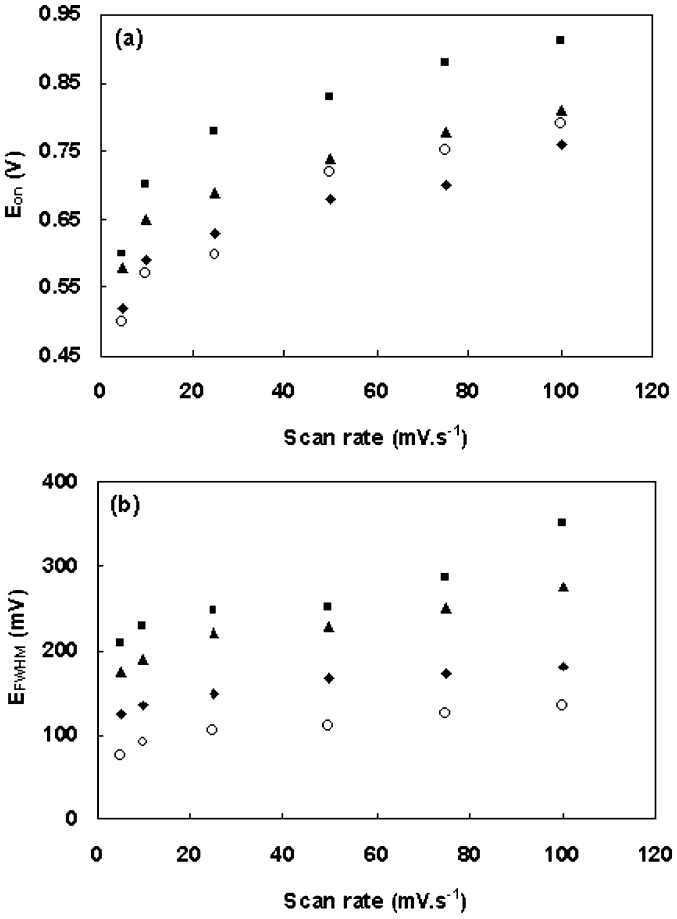


Fig. 8. Dependence of (a) the onset potential ($E_{on}$) and (b) the $E_{FWHM}$ values of the $CO_{ads}$ stripping reaction, respectively, on the sweep rate for the MWNT-g-PANI-Au (◆) (Au loading 40 μg cm$^{-2}$) and MWNT-g-PANI-Au electrode (○) (Au loading 60 μg cm$^{-2}$), MWNT-Au (▲) and pristine Au (■) electrodes.

A comparison of catalytic effect of oxidation of CO at MWNT-g-PANI-Au and MWNT-Au electrodes (with a similar loading of $Au^0$ nanoparticles) is also made. A $E_{FWHM}$ of about 75 mV is observed in the case of MWNT-g-PANI-Au electrode, whereas 175 mV is observed for MWNT-Au with a similar amount of $Au^0$ nanoparticles of 60 μg cm$^{-2}$. A narrow $CO_{ads}$ stripping peak and low $CO_{ads}$ oxidation potential (0.50 V) are also observed for the MWNT-g-PANI-Au ($Au^0$ nanoparticle loading of 60 μg cm$^{-2}$) electrode. However, in the case of MWNT-Au electrode, a partial beneficial effect is observed. In addition, the peak corresponding to the oxidation of $CO_{ads}$ is broader and expands into the more positive potential region than that observed for MWNT-g-PANI-Au. These results suggest that MWNT-g-PANI-Au electrode shows better oxidation kinetics for the oxidation of $CO_{ads}$ to $CO_2$ than the MWNT-Au and pristine Au electrodes. The presence of PANI as a grafted chain on the surface of MWNT not only disperses $Au^0$ particles more efficiently, but also provides increased electrocatalytic activity for the oxidation of CO. Such an increase can be attributed to different factors. The greater dispersion of $Au^0$ nanoparticles causes formation of smaller $Au^0$ particles, and hence increased formation of surface active sites that favor the adsorption of –OH species at lower potentials [49].

To understand the mechanism of CO oxidation at the MWNT-g-PANI-Au electrode, we studied the effect of scan rate on $CO_{ads}$ stripping peaks. We found that the sweep rate influenced the $CO_{ads}$ stripping characteristics at the electrode. Figs. 8a and b shows the dependence of the $E_{on}$ and $E_{FWHM}$ values for different sweep rates for the electrodes. Such behavior is well known [50] and indicates that the $CO_{ads}$ reaction is kinetically limited under the selected experimental conditions. A shift in the $E_{on}$ value toward a more positive potential and an increase in the $E_{FWHM}$ values with increasing sweep rate are observed for MWNT-g-PANI-Au electrodes (Figs. 8a and b). Over the entire range of sweep rates used in the study, the lowest $E_{on}$ values are observed for the MWNT-g-PANI-Au electrode. Moreover, the $E_{FWHM}$ values are smaller for the MWNT-g-PANI-Au electrode than for the MWNT-Au electrode. These observations indicate that oxidation of $CO_{ads}$ occurs comparatively faster at the MWNT-g-PANI-Au electrode. Overall, the MWNT-g-PANI-Au electrode exhibits better $CO_{ads}$ oxidation kinetics than the other electrodes, as is evident from its low $E_{on}$ and $E_{FWHM}$ values.

## 4. Conclusion

The newer catalysts comprising Au nanoparticles dispersed into PANI-grafted MWNT exhibit the essential characteristics, including enhanced electrocatalytic activities for methanol oxidation, restricted poisoning influence from adsorbed carbon monoxide, better oxidation kinetics, and performance at elevated temperatures, for use in DMFC applications. Our results demonstrate that the composite electrode consisting of MWNT, PANI, and $Au^0$ nanoparticles exhibit superior electrocatalytic activity compared with catalysts comprising MWNT and $Au^0$ nanoparticles and pristine Au electrode. The catalyst preparation method detailed in the present investigation is simple and provides future opportunities to use other conducting polymers and metal/alloy nanoparticles in generating other advanced catalysts for fuel cell applications and other devices.

## Acknowledgments

This work was supported by the Korean Research Foundation (grant KRF-2004-005-00009) and Brain Pool Program. The authors acknowledge the Korea Basic Science Institute (Deajon) and Kyungpook National University Center for Scientific Instruments.

## References

[1] B. Beden, C. Lamy, A. Bewick, L. Kunimatsu, J. Electroanal. Chem. 121 (1981) 343.
[2] A. Hamnett, Catal. Today 38 (1997) 445.
[3] A. Hamnett, in: Theory, Experiments and Applications, A. Wieckowski (Ed.), Dekker, New York, 1999, p. 843.
[4] G.T. Burnstein, C.J. Barnett, A.R. Kucernak, K.R. Williams, Catal. Today 38 (1997) 425.
[5] N. Lopez, J.K. Norskov, J. Am. Chem. Soc. 124 (2002) 11262.
[6] T.V. Choudhary, D.W. Goodman, Top. Catal. 21 (2002) 25.
[7] G.C. Bond, D.T. Thompson, Catal. Rev. 41 (1999) 319.

[8] T.F. Jaramillo, S.H. Baeck, B.R. Cuenya, E.W. McFarland, J. Am. Chem. Soc. 125 (2003) 7148.
[9] B. Beden, J.M. Leger, C. Lamy, in: J.O'M. Bockris, B.E. Conway, R.E. White (Eds.), in: Modern Aspects of Electrochemistry, vol. 22, Plenum Press, New York, 1992, Chapter 2.
[10] M. Haruta, M. Date, Appl. Catal. A 222 (2001) 427.
[11] M. Valden, X. Lai, D.W. Goodman, Science 281 (1998) 1647.
[12] J. Jia, K. Haraki, J.N. Kondo, K. Domen, K. Tamaru, J. Phys. Chem. B 104 (2000) 11153.
[13] M.M. Schubert, S. Hackenberg, A.C. van Veen, M. Muhler, V. Plzak, R.J. Behm, J. Catal. 197 (2001) 113.
[14] A. Wolf, F. Schuth, Appl. Catal. A 226 (2002) 1.
[15] H. Liu, A.I. Kozlov, A.P. Kozlova, T. Shido, K. Asakura, Y. Iwasawa, J. Catal. 185 (1999) 252.
[16] L.M. Bronstein, Top. Curr. Chem. 226 (2003) 55.
[17] G.C. Bond, Catal. Today 72 (2002) 5.
[18] M. Koudelka, J. Augustynski, J. Chem. Soc., Chem. Commun. (1983) 855.
[19] B. Beden, F. Hahn, J.M. Leger, C. Lamy, C.L. Perdriel, N.R. De Tacconi, R.O. Lezna, A.J. Arvia, J. Electroanal. Chem. 301 (1991) 129.
[20] C.A. Bessel, K. Laubernds, N.M. Rodriguez, R.T.K. Baker, J. Phys. Chem. B 105 (2001) 1115.
[21] A.A. Mikhaylova, O.A. Khazova, V.S. Bagotzky, J. Electroanal. Chem. 480 (2000) 225.
[22] A.A. Mikhaylova, E.B. Molodkina, O.A. Khazova, V.S. Bagotzky, J. Electroanal. Chem. 509 (2001) 119.
[23] I. Becerik, S. Suser, F. Kadirgan, J. Electroanal. Chem. 502 (2001) 118.
[24] S. Iijima, Nature 354 (1991) 56.
[25] J.M. Planeix, N. Coustel, B. Coq, V. Brotons, P.S. Kumbhar, R. Dutartre, P. Geneste, O. Bernier, P.M. Ajayan, J. Am. Chem. Soc. 116 (1994) 7935.
[26] H.C. Pham, N. Keller, L.J. Charbonniere, R. Ziessel, M. Ledou, Chem. Commun. (2000) 1871.
[27] C. Liang, Z. Li, J. Qiu, C. Li, J. Catal. 211 (2002) 278.
[28] G.L. Che, B.B. Lakshmi, E.R. Fisher, C.R. Martin, Nature 393 (1998) 346.
[29] S.H. Joo, S.J. Choi, I. Oh, J. Kwak, Z. Liu, O. Terasaki, R. Ryoo, Nature 412 (2001) 169.
[30] S.M. Golabi, A. Nozad, Electroanalysis 15 (2003) 278.
[31] T.C. Wen, Y.H. Chen, A. Gopalan, Mater. Chem. Phys. 77 (2002) 559.
[32] M.O. Finot, G.D. Braybrook, M.T. McDermott, J. Electroanal. Chem. 466 (1999) 234.
[33] W.C. Chen, T.C. Wen, C.C. Hu, A. Gopalan, Electrochim. Acta 47 (2002) 1305.
[34] G. Trejo, A.F. Gil, I. Gonzalez, J. Electrochem. Soc. 142 (1995) 3404.
[35] U. Schmidt, M. Donten, J.G. Osteryoung, J. Electrochem. Soc. 144 (1997) 2013.
[36] B. Xue, P. Chen, Q. Hong, J. Lin, K.L. Tan, J. Mater. Chem. (2001) 2378.
[37] R. Yu, L. Chen, Q. Liu, J. Lin, K.L. Tan, S.C. Ng, H.S.O. Chan, G.Q. Xu, T.S. Andy Hor, Chem. Mater. 10 (1998) 718.
[38] P.L.J. Gunter, J.W. Niemantsverdriet, F.H. Ribeiro, G.A. Somorjai, Catal. Rev. Sci. Eng. 39 (1997) 77.
[39] Joint Committee on Powder Diffraction Standards, Diffraction Data File, JCPDS International Center for Diffraction Data, Swarthmore, PA, 1991.
[40] M. Terrones, W.K. Hsu, A. Schilder, H. Terrones, N. Grobert, J.P. Hare, Y.Q. Zhu, M. Schwoerer, K. Prassides, H.W. Kroto, D.R.M. Walton, Appl. Phys. A 66 (1998) 307.
[41] L.V. Azaroff, Elements of X-Ray Crystallography, McGraw–Hill, New York, 1968, p. 549.
[42] S. Liu, Z. Tang, E. Wang, S. Dong, Electrochem. Commun. 2 (2000) 800.
[43] A. Dalmia, C.L. Lineken, R.F. Savinell, J. Colloid & Interface. 205 (1998) 535.
[44] T.S. Ahmadi, Z.L. Wang, T.C. Green, A. Henglein, M.A. El-Sayed, Science 272 (1996) 1924.
[45] T.S. Ahmadi, Z.L. Wang, A. Henglein, M.A. El-Sayed, Chem. Mater. 8 (1996) 1161.
[46] A.L. Santos, D. Profeti, P. Olivi, Electrochim. Acta. 50 (2005) 2615.
[47] M. Mastragostino, A. Missiroli, F. Soavi, J. Electrochem. Soc. 151 (2004) A1919.
[48] H.N. Dinh, X. Ren, F.H. Garzon, P. Zelenay, S. Gottesfeld, J. Electroanal. Chem. 491 (2000) 222.
[49] B.J. Kennedy, A. Hamnett, J. Electroanal. Chem. 283 (1990) 271.
[50] H.A. Gasteiger, N. Markovic, P.N. Ross, E.J. Cairns, J. Phys. Chem. 98 (1994) 617.